X-ray 2*p* photoelectron and L_α resonant x-ray emission spectra of the 3*d* metals in Ni_2MnZ (Z=In,Sn,Sb) Heusler alloys

M. V. Yablonskikh,[1,2] J. Braun,[3] M. T. Kuchel,[3] A. V. Postnikov,[2] J. D. Denlinger,[4] E. I. Shreder,[2] Y. M. Yarmoshenko,[2] M. Neumann,[5] and A. Moewes[1]

[1]*Department of Physics and Engineering Physics, University of Saskatchewan, Saskatoon, Canada S7N 5E2*

[2]*Institute of Metal Physics, Russian Academy of Sciences, Ural Division, 620219 Yekaterinburg GSP-170, Russia*

[3]*Physikalisches Institut, Westfälische-Wilhelms Universität Münster, Wilhelm-Klemm-Str. 10, D-48149 Münster, Germany*

[4]*Lawrence Berkeley National Laboratory, Berkeley, California 94720*

[5]*Department of Physics, Osnabrück University, D-49069 Osnabrück, Germany*

(Received 21 March 2006; published 1 August 2006)

Magnetic and chemical bonding effects in Heusler alloys Ni_2MnIn, Ni_2MnSn, and Ni_2MnSb were studied by soft x-ray spectroscopy. Exchange splitting detected in Mn 2*p* core-level x-ray photoelectron spectra and an increase of the Mn L_β/L_α intensity ratio in nonresonant x-ray emission spectra show that atomic magnetic moment at Mn is higher than that of pure metal. Spin polarized density of states calculations and comparative analysis of Mn and Ni L_α resonant x-ray emission spectra (RXES) demonstrate that the spin splitting in Mn 3*d* shell is larger than in Ni 3*d* shell. The *d*-*d* transitions observed in L_α RXES of Mn and Ni are suggested to be more intensive for Mn than for Ni valence electrons when initiated by off-resonant excitations. Experimental findings are supported by photoelectron spectra calculations and developed two-step model of resonant x-ray emission. The interplay between Mn L_α RXES and calculated magnetic moments of Mn atoms in alloys as a function of the type of *Z* element is discussed.

DOI: 10.1103/PhysRevB.74.085103 PACS number(s): 78.70.En, 75.50.Cc, 71.20.−b

I. INTRODUCTION

In 1903, Heusler alloys (HAs) were identified first as a special group of magnetic materials that exhibit ferromagnetism in compounds of nonmagnetic elements.[1] Currently, the Mn-based full Heusler alloys with the generic formula X_2MnZ (with *X* being a 3*d* metal and *Z* belonging to the III or IV group) are well known magnetic systems displaying the highest magnetic moment of up to $5\mu_B$ confined to manganese atoms. The magnetic moment of the second transition metal (X=Fe,Co,Ni,Cu) is approximately up to 10 times smaller, according to neutron scattering measurements[2,3] and band structure calculations.[4,5] Furthermore, the electronic structure of X_2MnZ alloys was predicted to significantly depend on the type of element *Z* due to the hybridization between *d*-*Y* and *p*-*Z* electronics states,[4,6] its concentration,[7] and the degree of crystallographic ordering.[8] The same trend is observed for T_c values where T_c is determined by the type of metal *X* for X_2MnZ while ΔT_c is changed as a function of *Z*, Ref. [3]. Understanding the interplay between local atomic moments and conduction electrons is important to comprehend diverse magnetic, optical and transport properties of these materials.

Applied research of Heusler alloys has been triggered up by the search for materials to be used as spin injectors.[9,10] The ideal material must be a ferromagnet with half-metallic band structure, i.e., the majority spin band is metallic while the minority spin band is semiconducting, along with a Curie temperature T_c high above room temperature.[11] Half-metallic band structure is an idealization[12] because of the decrease of spin polarization of spin carriers and vanishing of the semiconducting band gap for minority spin electrons in real crystals and interfaces caused by finite temperature effects and structural inhomogeneities.[13–15] Only some Heusler alloys are true half-metallic ferromagnets, but they possess other important properties. By varying element *Z* it is possible to tune the total band near the half-metallic state.[6,16,17] Despite the fact that T_c is close to room temperature, some Heusler alloys satisfy another criterium important to spin injectors—a small lattice mismatch with popular semiconductors, as for example Ni_2MnIn (6.072 Å) and InAs (6.058 Å).[18] It was predicted that the effective number of valence electrons can be controlled by the valence of atom *Z*.[6] It is known that magnetic properties of alloys are tied to the behavior of valence electrons of the atoms of their 3*d* metal constituents in alloys.[19] For Heusler alloys Mn and Ni 3*d* electrons are involved in valence to conduction band transitions along with *p* electrons of element *Z*.

We found an element specific signature of atomic magnetic moments in x-ray spectra of 3*d* metals in alloys. The interplay of Mn x-ray spectra with the atomic magnetic moment of Mn is discussed. We examined the magnitude of the spin splitting of Mn 3*d* electrons through the observation of *d*-*d* excitations in Mn RXES. The *d*-*d* excitations intensity is found to be dependent on element *Z* for the Mn RXES while Ni RXES do not show any dependence on *Z* element.

II. EXPERIMENTAL AND CALCULATIONAL DETAILS

A. X-ray spectroscopic transitions

We compare x-ray absorption, nonresonant x-ray photoelectron, nonresonant and resonant soft x-ray emission spectra further abbreviated in the text as XAS, NXPS, NXES, and RXES, respectively. X-ray photoelectron and x-ray absorption spectroscopies are first order optical processes. X-ray emission spectroscopy is a second-order optical process, in which the excited state decays by the fluorescence

transition of a valence electron to a core hole. Furthermore, it has to be noted that the intermediate state of the resonant x-ray emission process is the same as the final state of x-ray absorption, whereas that of x-ray fluorescence is the same as the final state of x-ray photoelectron emission.

A word about terminology is required to avoid the confusion in terms with that used in the literature. Here RXES are the result of superposition of the resonant elastic x-ray scattering (REXS) plus the resonant inelastic x-ray scattering (RIXS), which are also known within the x-ray Raman scattering,[20] and the x-ray fluorescence.[21] The contributions to a final spectrum are distinguished in the following way: the peak with the energy $\hbar\omega=\hbar\omega_0$ is an elastic peak representing REXS; a number of spectral features of varied intensity, which are the result of valence electron excitations, represent constant energy transfers $\hbar\omega_{\mathrm{loss}}$ from incoming photon to inelastically scattered one $\hbar\omega_{\mathrm{out}}=\hbar\omega_0-\hbar\omega_{\mathrm{loss}}$. As a result of changing the excitation energy, these loss features follow the elastic peak which corresponds to the energy $\hbar\omega_0$ in the photon energy scale. The third contribution to RXES are peaks of x-ray fluorescent transitions governed by the dipole selection rules.

For $3d$ metals it is convenient to utilize L_3 $(2p_{3/2}\rightarrow 3d)$ and L_2 $(2p_{1/2}\rightarrow 3d)$ excitations to probe d unoccupied conduction band states, and $L_{\alpha,\beta}$ $[(3d_{5/2,3/2}\rightarrow 2p_{3/2}),(3d_{3/2}\rightarrow 2p_{1/2})]$ x ray decays to probe d occupied valence band states. In $L_{3,2}$ XAS the transitions are $2p^63d^n4s^2+\hbar\omega_0\rightarrow 2p^53d^{n+1}4s^2$, where a $2p$ electron is excited to conduction band. This excitation is followed by a fluorescent $L_{\alpha,\beta}$ transition $2p^53d^{n+1}4s^2\rightarrow 2p^63d^n4s^2+\hbar\omega_{\mathrm{out}}$. Optically forbidden d-d excitations from the valence to conduction band $[2p^63d^n4s^2+\hbar\omega_0\rightarrow 2p^6(3d^n)^*4s^2+\hbar\omega_{\mathrm{out}}]$ may be observed in $L_{\alpha,\beta}$ resonant x-ray emission spectra. Atomic magnetic moments should be observable by means of x-ray photoelectron spectroscopy[22] and even by means of x-ray emission spectroscopy.[23]

B. Experimental measurements

The x-ray emission and absorption measurements were performed at the SXF Beamline 8.0.1 of the Advanced Light Source (ALS) at Lawrence Berkeley National Laboratory. The emitted radiation was measured using a Rowland-circle-type spectrometer with spherical gratings and a multichannel two-dimensional detector.[24] The instrumental resolution of the spectrometer was 1.0 eV. The energy bandwidth of the excitation beam was about 0.5 eV. The samples were filed in vacuum (1×10^{-6} Torr) before measurements. For the calibration of resonant x-ray emission spectra (RXES) we used reference spectra of pure metals and the energy values taken from Bearden *et al.*[25] XAS were measured in total electron yield mode (TEY) with resolution of 0.1 eV. Ni $2p$ NXPS for Ni_2MnZ (Z=In,Sn,Sb) have been measured with a PHI5600 ci-type ESCA spectrometer using monochromatized Al $K\alpha$ radiation with 0.3 eV bandwidth. The energy resolution of the analyzer was 1.5% of the pass energy. We estimate the energy resolution of the analyzer to be better than 0.35 eV. The pressure in the vacuum chamber during the measurements was below 3×10^{-9} mbar. The Mn $2p$ NXPS were measured at beamline 7.0.1 at the ALS. The Ni_2MnZ samples were fractured in a vacuum of better than 4×10^{-10} Torr. The excitation energy was selected to be 900 eV in order to measure the Mn $2p$ x-ray photoelectron spectra without contribution from the Ni Auger spectra that are present when exciting with Al $K\alpha$ radiation.[26] The energy resolution of the Mn $2p$ spectra was 0.3 eV, and for the valence band spectra it was 0.2 eV.

TABLE I. Essential parameters of measured spectra and calculated electronic structure of Ni_2MnZ. The B_R/A_R is a peak ratio for the case of the off-L_3 resonant excitation, see Fig. 9(b). Magnetic moments were calculated using WIEN2K (Ref. 27). The lattice constants are taken from Ref. 29.

Parameter	Ni_2MnIn	Ni_2MnSn	Ni_2MnSb	α-Mn
a (nm)	0.6072	0.6053	0.6000	
μ_{tot},μ_B	4.22	4.06	3.76	(1.9; 1.7; 0.6; 0.2)[a]
μ_{Ni},μ_B	0.35	0.24	0.17	
μ_{Mn},μ_B	3.44	3.45	3.37	
μ_Z,μ_B	−0.02	−0.02	−0.03	
B_R/A_R	0.96	0.87	0.62	

[a]It has to be noted that for four inequivalent manganese sites in metal and for manganese in Heusler alloys the experimental values of magnetic moment can vary, see Refs. 55 and 56, Refs. 3 and 30, and references therein.

C. Density of states calculations

Our band structure calculations were performed in the framework of the density functional theory, specifically, the full-potential augmented plane waves method, WIEN2K code[27] was used. The exchange-correlation potential was taken into account by the generalized gradient approximation after Perdew-Burke-Ernzerhof.[28] Calculations have been carried out for nominal experimental lattice constants, see Table I. Total and partial densities of states, further TDOS and PDOS, are calculated by the tetrahedron method with $14\times14\times14$ segmentations of the Brillouin zone.

The calculations shown in Figs. 1 and 2 are in good agreement with previously published results.[4,29,30] Also, experimental valence band (VB) photoelectron spectra presented in Fig. 3 are in good agreement with the literature.[26,31] For detailed element-specific analysis of the VB we point to Refs. 26 and 32. Here VB spectra of Ni_2MnZ alloys were used to validate the results of PDOS calculations shown in Fig. 1 are consistent with the measurements. The position of the valence band photoelectron spectra on the binding energy scale is in good agreement with that of maxima in calculated TDOS depicted in Fig. 2. The peak maxima of the valence band spectra of Heusler alloys follow the same trend as the peak maxima of TDOS distributions, which is a shift toward the Fermi level from Z=In and Sn to Sb. Presented TDOS calculations are found to be in good agreement with our VB measurements. Consequently our PDOS calculations are found valid.

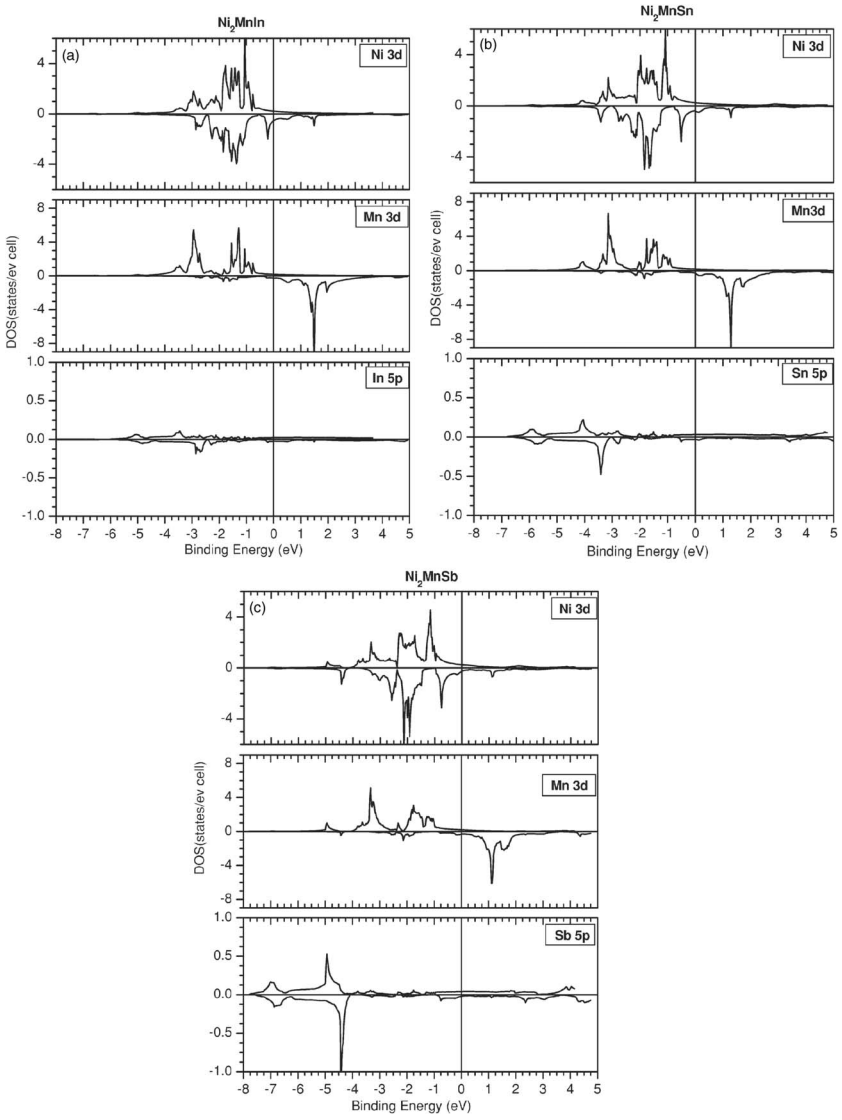

FIG. 1. Mn 3*d*, Ni 3*d*, and *Z p* spin-resolved partial densities of states in Ni_2MnIn, Ni_2MnSn, and Ni_2MnSb as calculated by WIEN2K (Ref. 27).

D. Two-step model of resonant x-ray emission

1. Theoretical method for RXES simulations

Calculations of the 3*d* metal RXES are not so straightforward. The majority of them is performed within the Anderson Impurity model[33] which has some limitations when applied to *f* and *d* electron metallic alloys (when comparing with semiconductors and ionic insulators).[20] Therefore we have developed a relatively simple time and momentum independent model valid for metallic alloys to calculate 3*d* RXES taken at excitation energies at the L_3 resonance and above L_3 threshold further labeled as off-L_3 resonant. The resonant character of the RIXS process is only evident at photon energies below the core-electron binding energy.[34] For L_3 and above L_3 threshold excitations the inelastically scattered contribution to L_α RXES cannot be separated from the fluorescent contribution because of the overlap in the photon energy.[35] In our simple approach, the RIXS contribution is replaced by a fluorescence decay imagining possible the x-ray emission both from the occupied and from the unoccupied part of the partial DOS.

A quantitative interpretation of the spectroscopic data needs a fully relativistic theory because spin-orbit coupling and exchange interaction in magnetic materials should be described with the same level of accuracy. For analysis we have developed a two-step model of the resonant x-ray emission process in the framework of relativistic multiple scattering theory.[36] In the first step a core hole is created with linearly polarized light of well defined frequency ω_0. If the energy of the radiation is sufficiently large, the electron is excited into the vacuum and can be described by a time-reversed low-energy electron diffraction (LEED) state. In this case a standard photoemission process takes place.[37] If the energy of the excited electron is below the vacuum energy E_V a different approach has to be chosen. Here we follow the idea of Hörmandinger *et al.*[38] that has been proven for example in the theoretical formulation of the Auger process. The Green function of the final state is described in

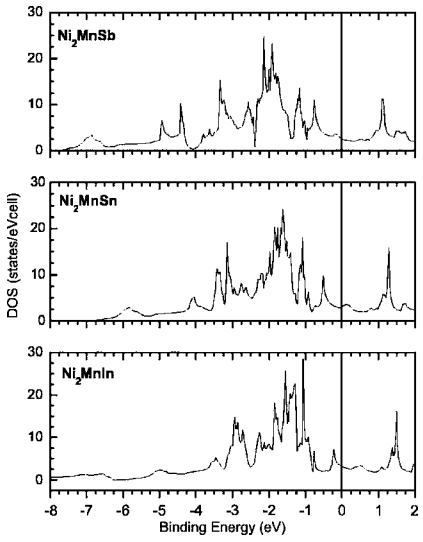

FIG. 2. Total density of states calculated using WIEN2K (Ref. 27).

terms of the bulk density of states (DOS) and the scattering solutions to the spin-polarized Dirac equation

$$\mathrm{Im}\, G(\mathbf{r},\mathbf{r}',E+\omega_0) \sim \sum_Q \frac{1}{2j+1} Z_Q(E+\omega_0,\mathbf{r}) n_Q(E+\omega_0) \times Z_Q(E+\omega_0,\mathbf{r}'). \quad (1)$$

Q denotes the relativistic quantum numbers $Q=(\kappa,\mu)$, n_Q being the local partial density of states (LDOS). The practical calculation of the single scattering solutions Z_Q was perfomed with the Dirac Hamiltonian h_{LDA} ($\hbar=m=e=1, c=137.036$) that results from the relativistic DFT[39,40]

$$h_{\mathrm{LDA}}(\mathbf{r}) = -ic\alpha\boldsymbol{\nabla} + \beta c^2 - c^2 + V_{\mathrm{LDA}}(r) + \beta\sigma\mathbf{B}_{\mathrm{LDA}}(r). \quad (2)$$

$V_{\mathrm{LDA}}(r)$ denotes the (effective) spin-independent potential, and $\mathbf{B}_{\mathrm{LDA}}(r)$ is the (effective) magnetic field. They are given as[41]

$$V_{\mathrm{LDA}}(r) = \frac{1}{2}[V^{\uparrow}_{\mathrm{LDA}}(r) + V^{\downarrow}_{\mathrm{LDA}}(r)],$$

$$\mathbf{B}_{\mathrm{LDA}}(r) = \frac{1}{2}[V^{\uparrow}_{\mathrm{LDA}}(r) - V^{\downarrow}_{\mathrm{LDA}}(r)]\mathbf{b}. \quad (3)$$

The constant unit vector **b** determines the spatial direction of the (uniform) magnetization as well as the spin quantization axis. β denotes the usual 4×4 Dirac matrix with the nonzero diagonal elements $\beta_{11}=\beta_{22}=1$ and $\beta_{33}=\beta_{44}=-1$, and the vector α is given by its components $\alpha_k=\sigma_x\otimes\sigma_k$ ($k=x,y,z$) in terms of the 2×2 Pauli matrices σ_k.

In both cases the excitation probabilities W_c for all core electrons under consideration can be calculated from

$$W_c(E+\omega_0) \equiv I_c^{\mathrm{XPS}}(E+\omega_0) \sim \mathrm{Im} \int d\mathbf{r} \int d\mathbf{r}' \Psi_c^*(\mathbf{r})\Delta^+(\mathbf{r}) \times G^F(\mathbf{r},\mathbf{r}',E+\omega_0)\Delta(\mathbf{r}')\Psi_c(\mathbf{r}'). \quad (4)$$

Ψ_c denotes a core state and Δ specifies the relativistic dipole operator in the electric dipole approximation which is well justified in the visible and ultraviolet spectral range. It mediates the coupling of the final state with the initial states. In a fully relativistic theory the dipole interaction of an electron with the electromagnetic field is given by the dipole operator $\Delta=-\alpha\mathbf{A}_0$, where $\mathbf{A}_0$ is the spatially constant vector potential inside the crystal. In a matrix element $\langle\Psi_f|\Delta|\Psi_i\rangle$ between eigenspinors $|\Psi_f\rangle$ and $|\Psi_i\rangle$ of the Dirac Hamiltonian with energies E_f and E_i, respectively, Δ follows to

$$\Delta = E_{fi}\left(\mathbf{A}_0\boldsymbol{\nabla} + \frac{i\omega}{c}\alpha\mathbf{A}_0\right)V_{\mathrm{LDA}} + E_{fi}(\mathbf{A}_0\boldsymbol{\nabla})\beta\sigma\mathbf{B}_{\mathrm{LDA}} + E_{fi}\frac{\omega}{c}\beta\mathbf{A}_0\times\sigma\mathbf{B}_{\mathrm{LDA}}, \quad (5)$$

with $E_{fi}=-2ic/[(E_f+c^2)^2-(E_i+c^2)^2]$. The expression is derived by making use of commutator and anticommutator rules.

The probabilities W_c will be used as weights to the XES intensities that are calculated for each core hole separately in a second step. This step involves the recombination of the core hole with a valence band electron. During this process radiation with a well defined frequency ω is emitted. Due to it's similarity to the photoemission process we adopt the same approach with some slight modifications. The XES intensities have been obtained from the following expressions:

$$I_c^{\mathrm{XES}}(E+\omega) \sim \mathrm{Im} \int d\mathbf{r} \int d\mathbf{r}' \Psi_c^*(\mathbf{r}) \times \Delta^+(\mathbf{r})G^I(\mathbf{r},\mathbf{r}',E+\omega)\Delta(\mathbf{r}')\Psi_c(\mathbf{r}'). \quad (6)$$

where I_c^{XES} is the XES intensity which is created due to the recombination of the core hole c. Since the Green function $G(\mathbf{r},\mathbf{r}',E+\omega)$ of the initial state denotes the electrons in the valence band, it is also necessary to have this quantity in terms of the DOS. Using Eq. (6) one can calculate the single

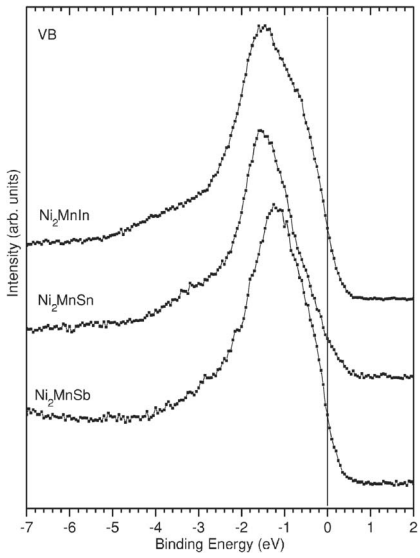

FIG. 3. Measured valence band photoelectron spectra of Ni_2MnZ alloys.

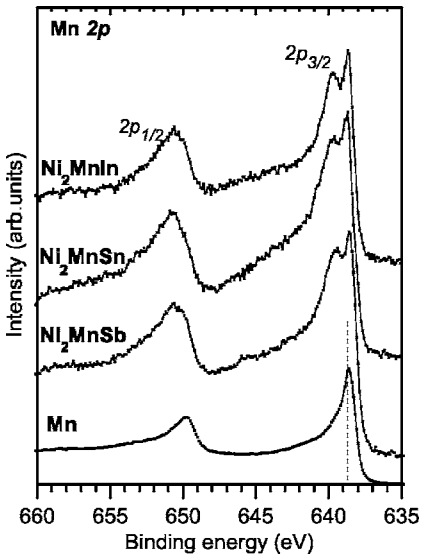

FIG. 4. Mn 2p X-ray photoelectron spectra of Heusler alloys. The spectrum of pure manganese is given for reference. The $2p_{3/2}$ core level binding energy of Mn in alloys is defined from the position of peak maxima which is labelled by a vertical dashed line.

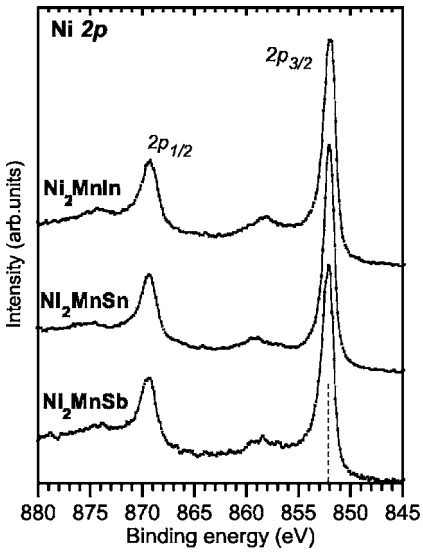

FIG. 5. Ni 2p XPS of Heusler alloys. The $2p_{3/2}$ core level binding energy of Ni (dashed line) is the same as in metal. The example of the spectrum of metallic Nickel is available in Ref. 54.

XES intensity for a specific core hole. The total RXES intensity is then obtained from the Kramers-Heisenberg formula[20] by a weighted superposition of the corresponding XES intensities using the W_c as weights:

$$I_{\omega_0}^{\mathrm{RXES}}(\omega) = \sum_c W_c \frac{I_c^{\mathrm{XES}}(\omega)}{(\omega-\omega_0)^2+\Gamma^2}. \tag{7}$$

Equation (7) represents a simple approach to the complicated resonant x-ray emission process. Nevertheless, we account for magnetic as well as for relativistic aspects on the same level of accuracy by using relativistic multiple scattering techniques for calculating the weights W_c and the XES intensities. Furthermore we account quantitatively for the bulklike emission process when applying multiple scattering theory to the excitation process.

2. Computational details

The model has been been applied to the spectroscopic analysis of the three Mn-based Heusler alloys Ni_2MnIn, Ni_2MnSn, and Ni_2MnSb probing their corresponding electronic and magnetic properties. The electronic structure of the three Heusler alloys has been calculated by the linear muffin-tin orbitals method[42] in its tight binding implementation.[43] The spin-dependent potentials together with the corresponding spin-resolved DOS's serve as input quantities for the theoretical RXES intensity distributions.

For the off-L_3 resonant case we used W_c calculated by the method used for XPS calculations.[37] For the L_3 resonant case a modified photoemission procedure was applied to calculate W_c. In this case the electrons from the Mn 2p core states are excited into the conduction band just above the Fermi level, causing the empty states to be partially filled. To simulate this process we used again the DOS, which was employed for the calculation of the weights W_c, but the Fermi level has been shifted to higher energies. The shift S_F of the Fermi level was adjusted so that good agreement between the experimental and theoretical spectra has been achieved. Damping processes have been accounted for in a phenomenological way choosing Γ as a constant in energy but with different values for the different alloys. The corresponding values for Γ and S_F are presented in Table II. The calculated spectra have been shifted until the experimental and theoretical peak maxima coincide. The theoretical core-level energies are −605.5, −609.2, and −608.5 eV for Mn $2p_{3/2}$ in Ni_2MnSn, Ni_2MnIn, and Ni_2MnSb, respectively. The values for ω_0^R given in Table II represent the sums of the negative core-level binding energies with the Fermi energies of the corresponding Heusler alloy. For the off-L_3 resonant case we decided to add to ω_0^R a value of 4.0 eV, so that the excitation with ω_0^{NR} puts the electron into the vacuum. In other words we were able to apply the XPS formalism for the excitation step. As one would expect, in this case only a slight shift of the Fermi-level was necessary to achieve a good agreement with the experimental data. To take into account for experimental broadening, all calculated spectra were convoluted with Gaussians of full width at half maximum=1.2 eV.

III. DISCUSSION

A. Nonresonant 2p XPS and $L_{\alpha,\beta}$ XES

The 2p core-level XPS of 3d metals of Heusler alloys are shown in Figs. 4 and 5. Similar to Mn 2p XPS, Mn $L_{\alpha,\beta}$ NXES depicted in Fig. 6 demonstrate differences to the metallic references, in particular in the L_β/L_α peak ratio. This is in contrast to the data for Ni shown in Fig. 7. The large magnetic moment of about $3-4\mu_B$ attributed to the Mn sites and the small magnetic moment of less than $0.4\mu_B$ associated with the Ni sites are in good agreement with appearance of

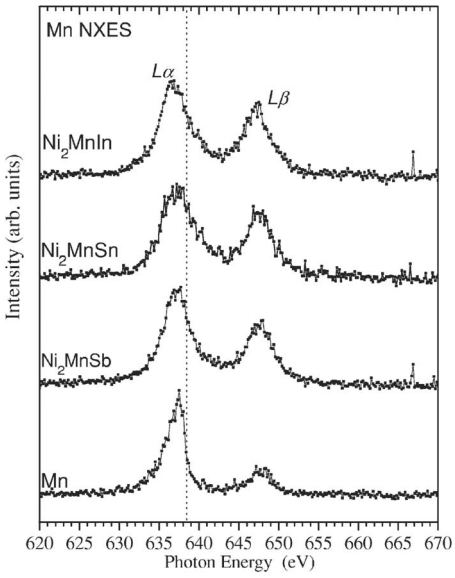

FIG. 6. Mn $L_{\alpha,\beta}$ NXES. The vertical dotted line corresponds to the Mn $2p_{3/2}$ core level binding energy taken from Fig. 4.

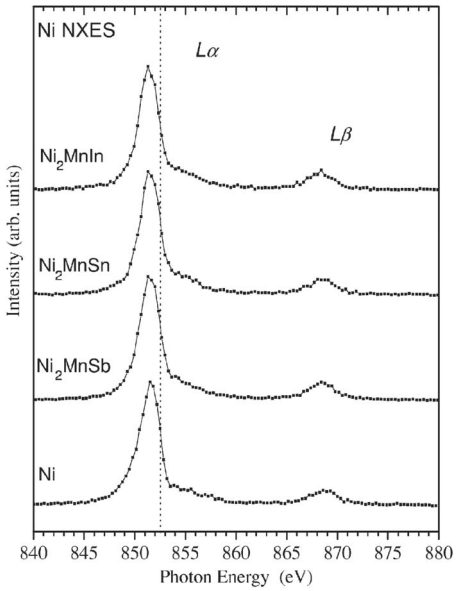

FIG. 7. Ni $L_{\alpha,\beta}$ NXES. The vertical dotted line corresponds to the Ni $2p_{3/2}$ core level binding energy taken from Fig. 5.

these effects for Mn and absence of such in Ni in alloys. The origin of these differences from the spectra of metallic references is known to be magnetic.[22,26] According to calculations[44] the $2p_{3/2}$ and $2p_{1/2}$ exchange splitting of Mn and Co $2p$ NXPS for Co_2MnSn compounds increases following the calculated increase of Co and Mn magnetic moments as a function of the a lattice parameter. These changes are small. For example, $\Delta\mu_{Mn}=0.2\mu_B$ corresponds to the core level energy splitting of $\Delta E_{2p_{3/2},Mn}=0.08$ eV and $\Delta\mu_{Co}=0.04\mu_B$ corresponds to $\Delta E_{2p_{3/2},Co}=0.02$ eV.[44]

The Mn $2p$ calculated XPS is shown in Fig. 8. The shape of the computed NXPS changes with the atomic number of the Z element while the magnitude of the peak splitting remains close to constant. The result is that the correlation between the $2p_{3/2}$ core level energy splitting and the value of atomic magnetic moment of manganese in alloys is valid in theory, but it is difficult to be confirmed experimentally. The corresponding changes of the calculated values of μ_{Mn} are very small, see Table I. They are found to be within the error which may reach up to $0.10-0.11\mu_B$.[45] Introduced crystal defects may increase the margins for the μ_{Mn} up to $0.5\mu_B$ (Ref. 45) which is similar to experimental observations (see, for example, Ref. 3, and therein). As for Mn $2p$ XPS, no

TABLE II. Values of the damping constant Γ and the Fermi level shift S_F for Mn-based Heusler alloys for resonant (ω_0^R) and nonresonant (ω_0^{NR}) excitation from the Mn-$2p_{3/2}$ core levels.

	Ni_2MnIn	Ni_2MnSn	Ni_2MnSb
ω_0^{NR} (eV)	621.90	619.30	621.90
Γ^{NR} (eV)	0.50	0.50	0.50
S_F^{NR} (eV)	0.35	0.20	−0.20
ω_0^R (eV)	617.90	615.30	617.90
Γ^R (eV)	0.17	0.17	0.24
S_F^R (eV)	0.80	0.80	2.50

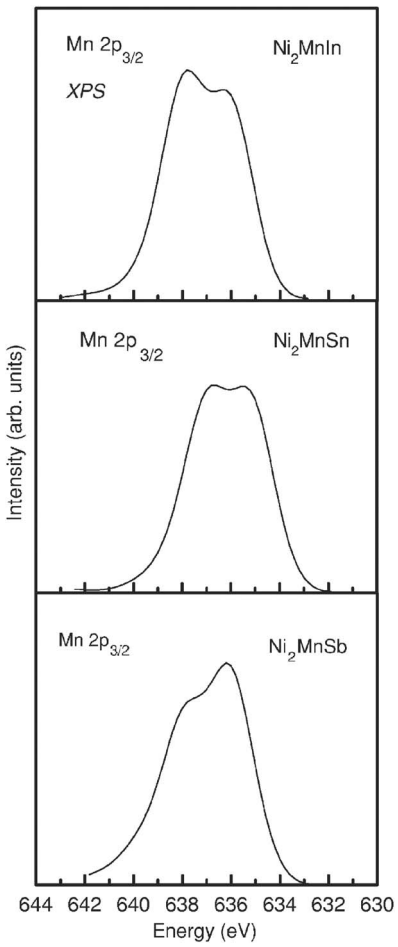

FIG. 8. Calculated Mn $2p$ x-ray photoelectron spectra of Heusler alloys.

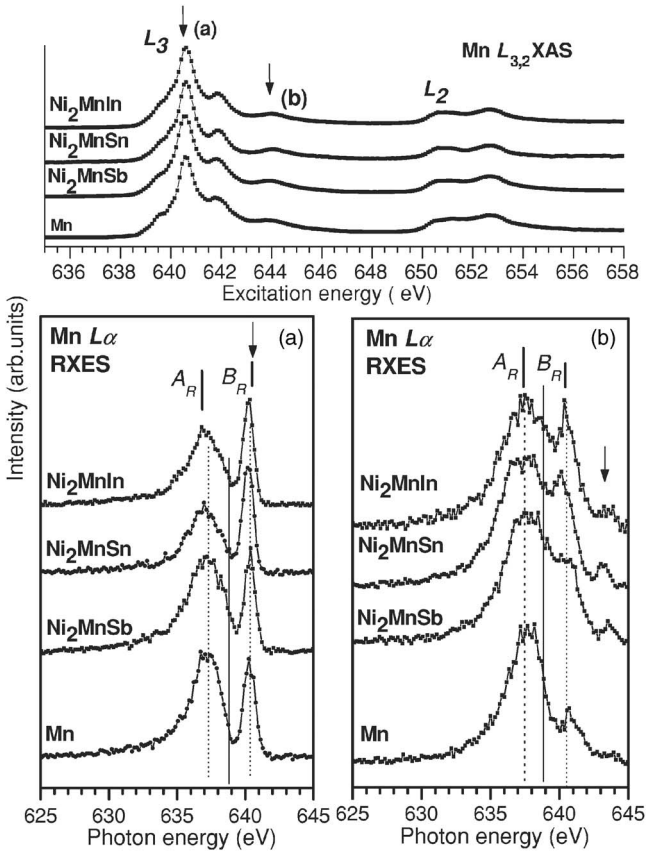

FIG. 9. Mn $L_{2,3}$ XAS (top frame) and L_α RXES of Heusler alloys and of elemental Mn (bottom frame) are shown at the left graph. The positions of the two excitation energies, one corresponding to the L_3 resonance (a) and off-L_3 resonance (b), are labeled by arrows in the corresponding XAS. The Mn L_α resonant x-ray emission spectra of alloys and elemental metal excited at the energies (a) and (b) are shown in the two separate panels labeled (a) and (b). The Mn $2p_{3/2}$ core level binding energy taken from Fig. 4 is indicated by a vertical line. Each of Mn L_α RXES is assumed to consist from two peaks A_R and B_R. Positions of these peaks in the photon energy scale are defined by the primary maxima in spectra. They are marked by dotted lines.

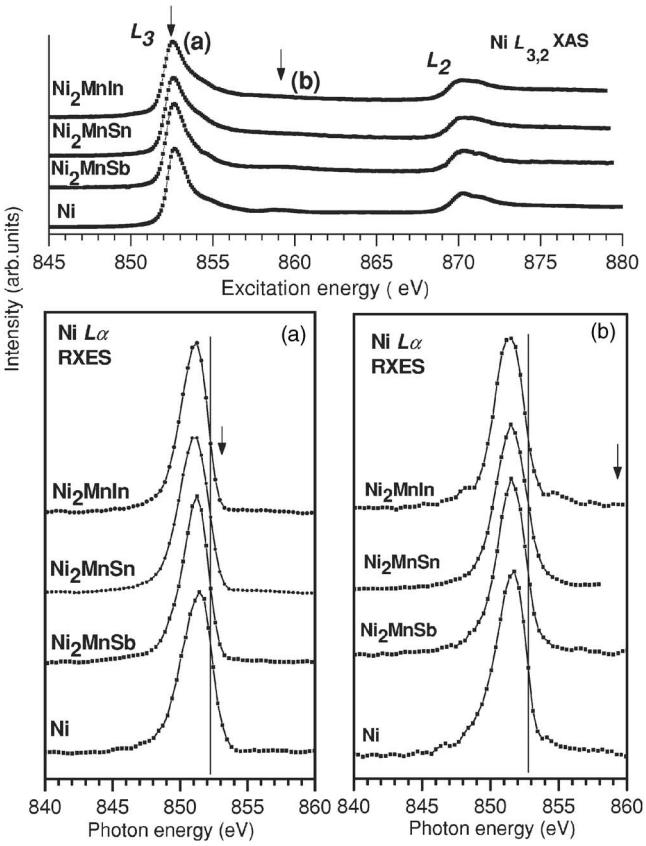

FIG. 10. Ni $L_{2,3}$ XAS (top frame) and L_α RXES of Heusler alloys and of elemental Ni (bottom frame) are shown at the left graph. All designations are the same as in Fig. 9.

agreement between the Mn L_β/L_α intensity ratio and the magnitude of the calculated magnetic moments of Mn as a function of the element Z is observed for Ni_2MnZ alloys. The increase of the Mn L_β/L_α intensity ratio relative to that for Mn is shown in Fig. 6. A suggested explanation was a modification of the dipole selection rules for Mn $L_{\alpha,\beta}$ XES.[26] However, this ratio may be altered, for example, by Coster-Kronig transitions resulting in a satellite structure at the high energy side of L_α spectrum.[46] This satellite contribution located above the binding energy of 2p core level is more pronounced for Mn L_α NXES as compared for Ni NXES. Therefore, it is better to analyze $3d \rightarrow 2p$ transitions directly without the satellite effects caused by excitations with energies well above the L_2 absorption threshold. This is will be done in the following section.

Even remain unexplained, both the appearance of the core level energy splitting $\Delta E_{2p_{3/2}}$ in NXPS and the L_β/L_α intensity ratio in NXES of higher than that in reference metal indicate the degree of spin polarization of Mn 3d electrons to be larger than that of Ni 3d in Heusler alloys. We note that the magnetic moment effects in soft x-ray spectra are observable once μ_{TM} becomes larger than $2\mu_B$.[47] Therefore, in our investigation of magnetic effects, we will discuss further only the data obtained for Mn.

B. 3d metal L_α RXES

$L_{\alpha,\beta}$ RXES, 2p NXPS, and $L_{\alpha,\beta}$ NXES are similar in the following sense: small spectral differences were found in the Ni spectra of Heusler alloys and metallic Ni while Mn spectra exhibit pronounced differences from the metallic reference. The Mn L_α and Ni L_α RXES depicted in Figs. 9 and 10, respectively, were each acquired at L_3 resonant (a) and off-L_3 resonant (b) excitation energies. We analyze features A_R and B_R in Mn L_α RXES, whose peak positions in the photon energy scale remain the same for all three compounds.

According to PDOS calculations shown in Fig. 1, for Mn 3d states the spin-up and spin-down bands are split below and above the Fermi energy, respectively. The Mn 3d DOS shows maxima at binding energies of −3 and −1 eV for majority spin DOS and at 1.5 eV for minority spin DOS. From the comparison between the total DOS (see inset in Fig. 11) and the spin-polarized partial DOS (Fig. 1) of Ni_2MnSb we

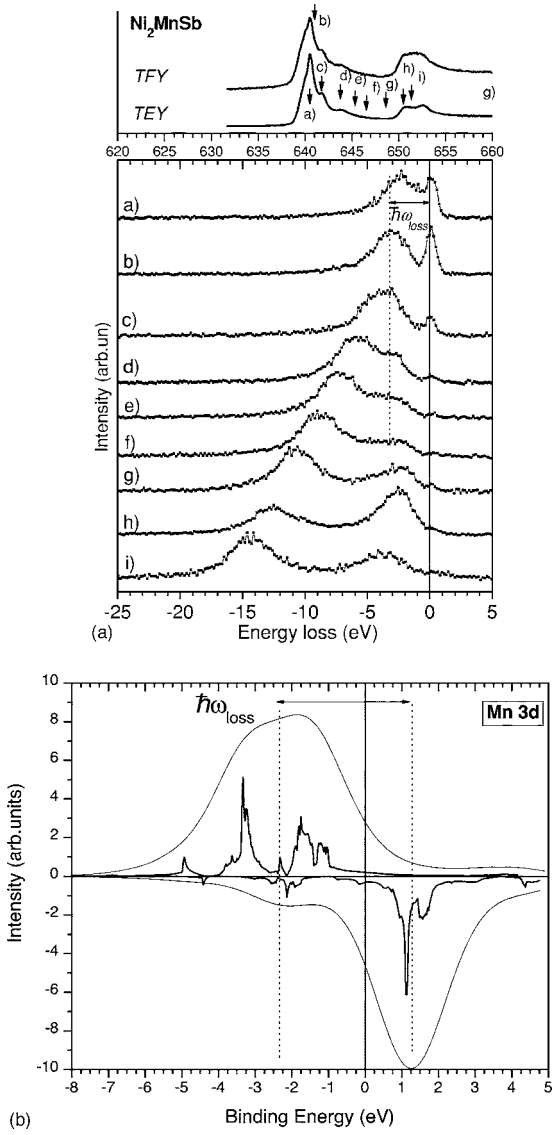

FIG. 11. Mn $L_{\alpha,\beta}$ Top frame: X-ray emission in the energy loss scale. Bottom frame: The Mn $3d$ DOS and its convolution with Gaussians to fit experimental resolution.

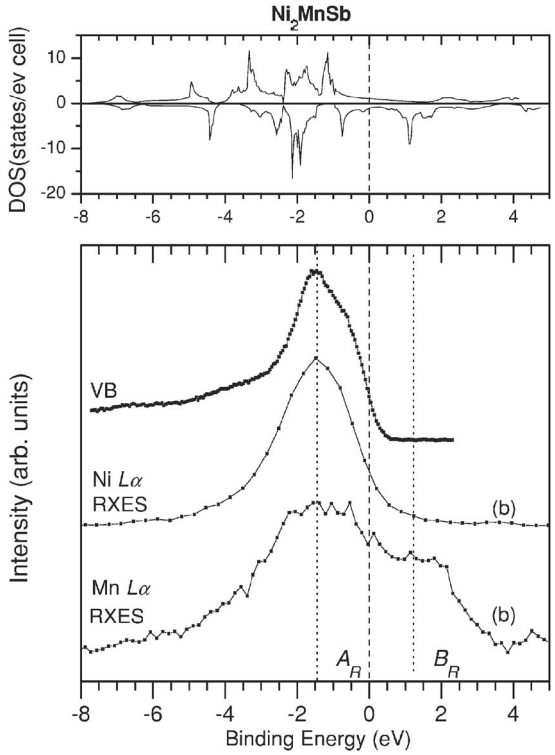

FIG. 12. The experimental valence band spectrum Mn L_α and Ni L_α RXES and spin-polarized total DOS calculations in the binding energy scale. The Mn L_α and Ni L_α RXES were taken for the case of the off-L_3 resonant excitation (b) from Figs. 9 and 10, respectively. The position of the Fermi energy at the ground state is defined by the $2p_{3/2}$ binding energies taken from Figs. 4 and 5. The spin-polarized total DOS is calculated by WIEN2K (Ref. 27).

also see that the conduction spin-down states are mostly due to Mn. The RIXS contribution B_R to Mn L_α RXES of Heusler alloys represent d-d net transitions of the kind $2p^6 3d^5 4s^2 \rightarrow 2p^6 (3d^5)^* 4s^2$ where a d electron is excited from the states below the Fermi level to unoccupied states. Mn L_α RXES shown in Fig. 11 exhibit a loss feature at the energy $\hbar\omega_{\text{loss}}$ following the elastic peak as observed for excitation energies from (a) to (f). Neglecting momentum conservation we map Mn L_α RXES and the Mn $3d$ DOS of Ni_2MnSb. The $\hbar\omega_{\text{loss}}$ energy corresponds quite well to the energy separation between the local maxima in the occupied and unoccupied Mn $3d$ DOS as shown in the inset to Fig. 11. We note that the energy resolution of Mn RXES (see Sec. II B) is not enough to clearly distinguish d states which correspond to many different d-d excitations. However, one can say that the high energy satellite in Mn L_α RXES [marked as peak B_R in Fig. 9(b)] appears primarily due to d-d excitations in contrast to $3d \rightarrow 2p$ fluorescence as proposed before.[48] Comparing the selected off-L_3 resonantly excited data for Mn and Ni with the tDOS calculations shown in Fig. 12, we assume that the probability of the d-d excitation is higher for Mn atoms in comparison with Ni atoms. Due to almost 100% spin splitting of the Mn $3d$ electrons, it is obvious that Mn these d-d transitions are accompanied by spin flip[50,51,58] as a result of core electron photoionization.[53]

From the comparison shown in Fig. 12 for Ni_2MnSb, one can see that the Mn L_α, displayed on the binding energy scale, is more broader than Ni L_α RXES. The position of Mn and Ni RXES was defined neglecting the effect of the $2p$ core hole from the $2p_{3/2}$ Mn and Ni NXPS (Figs. 4 and 5), respectively. In contrast to the situation with Ni L_α RXES, E_F splits the Mn L_α into two parts. The full width at half maximum of the peak B_R located above E_F is about 1–1.5 eV and the width of the peak below E_F is approximately at −(3–3.5) eV. The result is in transparent agreement with the PDOS calculations shown in Fig. 1. In contrast to Mn, the Ni atoms exhibit only a weak spin splitting of their $3d$ states. Surprisingly the energy difference between features A_R and B_R is in good agreement with the Mn $3d$ convoluted spin-up and spin-down maxima of PDOS. Supported by x-ray photoelectron measurements for Ni_2MnZ alloys the $3d$ metal RXES data show a stronger spin polarization of the Mn $3d$ electrons than those for Ni in alloys and Mn in metallic form.

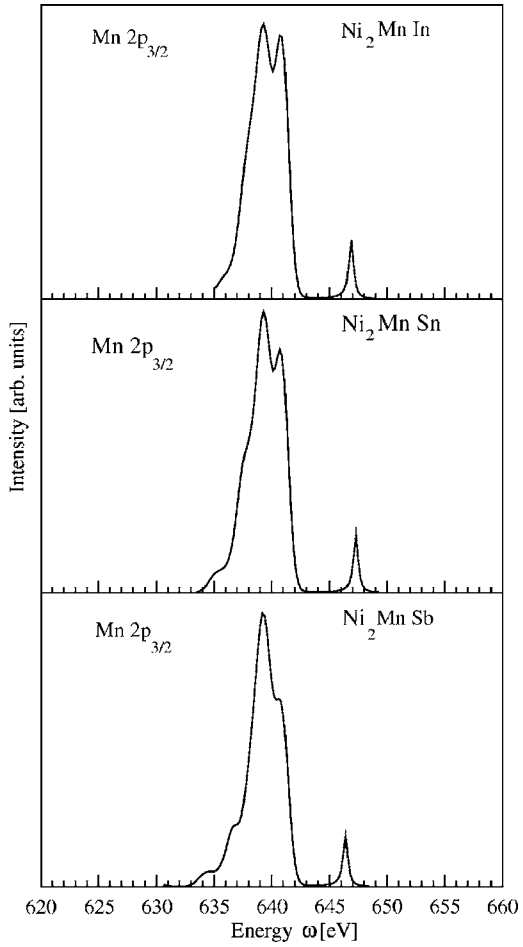

FIG. 13. Off-resonant x-ray emission spectra calculated for Mn $2p_{3/2}$ core-level excitation from three different Heusler alloys. The excitation energy ω_0^{NR} corresponds to label (b) in Fig. 9.

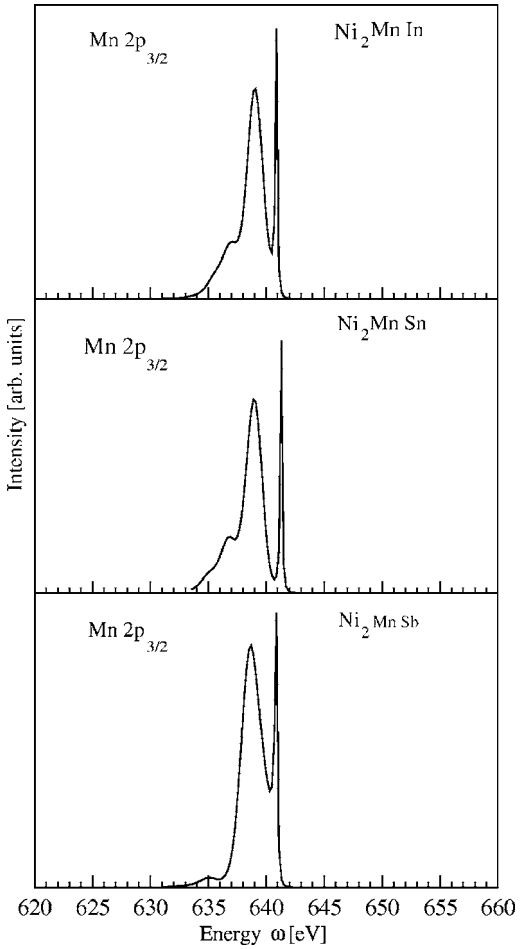

FIG. 14. Resonant x-ray emission spectra calculated for Mn $2p_{3/2}$ core-level excitation from three different Heusler alloys. The excitation energy ω_0^R corresponds to label (a) in Fig. 9.

C. Comparison between theory and experiment

It turned out that the one-particle approach with the time independent treatment works well for numerical calculations of 3d metals RXES[48] and even NXES.[49] Resonant and nonresonant x-ray emission spectra for three different Heusler alloys have been investigated within the formalism that has been discussed in the previous section. The off-L_3 resonant case is shown in Fig. 13. At the top of Fig. 13 the Mn L_α spectrum for Ni_2MnIn is shown. The pronounced double peak structure at about 640 eV can be ascribed to the occupied Mn majority d states. The second peak located at 647 eV represents the strongly decreased intensity of the inelastic peak that is shifted to a higher energy in accordance with the value for ω_0^{NR}. The calculated double peak structure coincides with the two experimental peaks A_R and B_R in Fig. 9. Both the intensities and the energetic positions are well described by the theory. Due to our choice of ω_0^{NR} the resonancelike feature, marked in the experimental data by a down arrow, is found at the measured energetic position. Also an appropriate value for the damping constant Γ guarantees a relative intensity of this peak that is in quantitative agreement with the experiment. Going to Ni_2MnSn the double peak structure turns out to be less pronounced. This is again in good agreement with the measurements and in consequence tells us that the calculated partial density of states for Mn in these Heusler alloys is well described by a density functional calculation in the local density approximation. The peak labeled by B_R further decreases in intensity whereas the other peaks remain more or less constant. This behavior reflects mostly the evolution of the Mn majority LDOS due to the substitution of Sn and Sb for In in the alloy.

The situation changes dramatically for the resonant L_3 case because the intermediate states now play an important role. This is clearly visible in Fig. 14 where the calculated resonant x-ray emission spectra are shown. In accordance with the experimental data the double peak structure at about 640 eV completely vanishes. Instead we observe a strongly enhanced resonance peak at 641 eV. The total width of the spectral distributions as well as the positions of the different peaks have been obtained at the same level of agreement with the experiment we found in the off-L_3 resonant case. Surprisingly, good agreement between experiment and theory has been achieved within the simple two-step model in combination with a reasonable parametrization of the spectral distributions. The simulation of the intermediate state by only shifting the Fermi level to higher energies shows that for some intermetallic alloys the single-particle

picture works quite well, even if *d* states are involved.

The full Heusler alloys show a Slater-Pauling behavior where the total spin magnetic moment per unit cell linearly scales with the total number of valence electrons linearly.[6] The decrease of the B_R/A_R ratio, which is in good agreement with the increase of PDOS below the E_F for element *Z*, is due to *p*-*Z*–*d*-Mn hybridization.[50] We note that the drop of B_R/A_R peak ratio for off-L_3 resonant excitation from the Mn L_α RXES from *Z*=In,Sn to *Z*=Sb is in good agreement with an estimated decrease of μ_{Mn}. The calculated magnetic moments are 3.44, 3.45, and 3.37 μ_B for *Z*=In,Sn,Sb, respectively. The trend for these values coincides also with the phenomenologically selected values for Γ^R (Table II: 0.17, 0.17, and 0.24). Thus, we suggest that for off-L_3 excitation the Mn L_α RXES may directly correlate with the magnitude of μ_{Mn}. However, similar to the conclusion made from the 2*p* XPS analysis in Sec. III A, the correlation between the Mn L_α RXES and the experimental values of the μ_{Mn} as a function of *Z* element cannot be declared due to the mentioned error margins in experimental measurements of μ_{Mn} found in the literature.

IV. CONCLUSIONS

Nonresonant 2*p* core level x-ray photoelectron and $L_{\alpha,\beta}$ fluorescent spectroscopy may be used to identify the presence of large atomic magnetic moments and evaluate the degree of spin polarization of the 3*d* electrons of *d* metal constituents in Heusler alloys. From the comparison between the Mn L_α and Ni L_α RXES it is evident that *d*-*d* excitations are more intensive for Mn atoms than Ni atoms. Moreover, *d*-*d* excitation probability at Mn sites is found to be dependent on the *Z* element. The changes in atomic magnetic moment of 3*d* metal constituent are expected to be observed through experiment for the family of X_2Mn*Z* alloys when the element *Z* is substituted.

Proposed correlation between the experimental XPS and RXES and the values of atomic magnetic moments as a function of the element *Z* requires further investigation. An adequate theoretical support is welcomed. Further, we note that similar experiments using circularly polarized light in resonant x-ray photoelectron emission, x-ray photon absorption, and emission spectroscopy will provide a better insight into spin dynamics.[57]

ACKNOWLEDGMENTS

The authors would like to thank Kai Rossnagel, beamline 7.0.1, for experimental support and Mikhail Katsnelson for insightful discussion. Funding from the Natural Sciences and Engineering Research Council of Canada (NSERC) is gratefully acknowledged. The work at the Advanced Light Source at Lawrence Berkeley National Laboratory was supported by U.S. Department of Energy (Contract No. DE-AC03-76SF00098).

[1] F. Heusler, Verh. Dtsch. Phys. Ges. **5**, 219 (1903).
[2] K. R. A. Ziebeck and K.-U. Neumann, *Magnetic Properties of Metals*, Vol. 32/c of Landolt-Börnstein New Series, Group III (Springer-Verlag, Berlin, 2001), pp. 66–414.
[3] P. Webster and K. Ziebeck, *Alloys and Compounds of d-elements with Main Group Elements*, Landolt-Börnstein, Part 2, Vol. 19, New Series, Group III (Springer-Verlag, Berlin, 1988), pp. 75–184.
[4] J. Kübler, A. R. Williams, and C. B. Sommers, Phys. Rev. B **28**, 1745 (1983).
[5] I. Galanakis, P. H. Dederichs, and N. Papanikolaou, Phys. Rev. B **66**, 134428 (2002).
[6] I. Galanakis, P. H. Dederichs, and N. Papanikolaou, Phys. Rev. B **66**, 174429 (2002).
[7] S. Fujii, S. Ishida, and S. Asano, J. Phys. Soc. Jpn. **63**, 1881 (1994).
[8] B. Ravel, J. O. Cross, M. P. Raphael, V. G. Harris, R. Ramesh, and V. Saraf, Appl. Phys. Lett. **81**, 2812 (2002).
[9] P. R. Hammar, B. R. Bennett, M. J. Yang, and M. Johnson, Phys. Rev. Lett. **83**, 203 (1999).
[10] G. A. Prinz, Science **282**, 1660 (1998).
[11] R. A. de Groot, F. M. Mueller, P. G. van Engen, and K. H. J. Buschow, Phys. Rev. Lett. **50**, 2024 (1983).
[12] P. A. Dowben and R. Skomski, J. Appl. Phys. **95**, 7453 (2004).
[13] R. J. Soulen, Jr, J. M. Byers, M. S. Osofsky, B. Nadgorny, T. Ambrose, S. F. Cheng, P. R. Broussard, C. T. Tanaka, J. Nowak, J. S. Moodera, A. Barry, and J. M.D. Coey, Science **282**, 85 (1998).
[14] M. P. Raphael, B. Ravel, M. A. Willard, S. F. Cheng, B. N. Das, R. M. Stroud, K. M. Bussmann, J. H. Claassen, and V. G. Harris, Appl. Phys. Lett. **79**, 4396 (2001).
[15] P. J. Brown, K. U. Neumann, P. J. Webster, and K. R. A. Ziebeck, J. Phys.: Condens. Matter **12**, 1827 (2000).
[16] S. Ishida, S. Fujii, S. Kawhiwagi, and S. Asano, J. Phys. Soc. Jpn. **64**, 2152 (1995).
[17] S. Fujii, S. Ishida, and S. Asano, J. Phys. Soc. Jpn. **64**, 185 (1995).
[18] K. A. Kilian and R. H. Victora, J. Appl. Phys. **87**, 7064 (2000).
[19] D. Goodenough, *Magnetism and Chemical Bonding* (Interscience Publishers, New York, 1963).
[20] A. Kotani and S. Shin, Rev. Mod. Phys. **73**, 203 (2001).
[21] A. Kotani, J. Electron Spectrosc. Relat. Phenom. **92**, 171 (1998).
[22] Y. M. Yarmoshenko, M. I. Katsnelson, E. I. Shreder, E. Z. Kurmaev, A. Slebarski, S. Plogmann, T. Schlatholter, J. Braun, and M. R. Neumann, Eur. Phys. J. B **2**, 1 (1998).
[23] J. Badro, G. Fiquet, F. Guyot, J. P. Rueff, V. V. Struzhkin, G. Vanko, and G. Monaco, Science **300**, 789 (2003).
[24] J. J. Jia, T. A. Callcott, J. Yurkas, A. W. Ellis, F. J. Himpsel, M. G. Samant, J. Stohr, D. L. Ederer, J. A. Carlisle, E. A. Hudson, L. J. Terminello, D. K. Shuh, and R. C. C. Perera, Rev. Sci. Instrum. **66**, 1394 (1995).
[25] J. A. Bearden, Rev. Mod. Phys. **39**, 78 (1967).
[26] S. Plogmann, T. Schlatholter, J. Braun, M. Neumann, Y. M. Yarmoshenko, M. Yablonskikh, E. I. Shreder, E. Z. Kurmaev, A.

Wrona, and A. Slebarski, Phys. Rev. B **60**, 6428 (1999).
[27] P. Blaha, K. Schwarz, G. K. H. Madsen, D. Kvasnicka, and J. Luitz, WIEN2K, Vienna University of Technology, 2001, improved and updated UNIX version of the original copyrighted WIEN code, which was published by P. Blaha, K. Schwarz, P. Sorantin, and S. B. Trickey, Comput. Phys. Commun. **59**, 339 (1990).
[28] J. P. Perdew, K. Burke, and M. Ernzerhof, Phys. Rev. Lett. **77**, 3865 (1996).
[29] E. Z. Da Silva, O. Jepsen, and O. K. Andersen, Solid State Commun. **67**, 13 (1988).
[30] E. Sasioglu, L. M. Sandratskii, and P. Bruno, Phys. Rev. B **70**, 024427 (2004).
[31] S. W. Robey, L. T. Hudson, and R. L. Kurtz, Phys. Rev. B **46**, 11697 (1992).
[32] D. Brown, M. D. Crapper, K. H. Bedwell, M. T. Butterfield, S. J. Guilfoyle, A. E. R. Malins, and M. Petty, Phys. Rev. B **57**, 1563 (1998).
[33] P. Anderson, Phys. Rev. B **124**, 41 (1961).
[34] M. Magnuson, J. E. Rubensson, A. Fohlisch, N. Wassdahl, A. Nilsson, and N. Martensson, Phys. Rev. B **68**, 045119 (2003).
[35] J. P. Briand, D. Girard, V. O. Kostroun, P. Chevallier, K. Wohrer, and J. P. Mosse, Phys. Rev. Lett. **46**, 1625 (1981).
[36] J. Korringa, Physica (Amsterdam) **6/7**, 392 (1947); W. Kohn and N. Rostocker, Phys. Rev. **94**, 1111 (1954); K. Kambe, Z. Naturforsch. A **22**, 322 (1967); A. R. Williams and J. van Morgan, J. Phys. C **7**, 37 (1974); R. G. Brown and M. Ciftan, Phys. Rev. B **27**, 4564 (1983); X.-G. Zhang, A. Gonis, and J. M. MacLaren, *ibid.* **40**, 3694 (1989); W. H. Butler and R. K. Nesbet, *ibid.* **42**, 1518 (1990); H. Ebert and B. L. Gyorffy, J. Phys. F: Met. Phys. **18**, 451 (1988); S. C. Lovatt, B. L. Gyorffy, and G. Y. Guo, J. Phys.: Condens. Matter **5**, 8005 (1993); R. Feder, J. Phys. C **14**, 2049 (1981).
[37] J. Braun, in *Band-Ferromagnetism: Ground-State and Finite-Temperature Phenomena*, edited by K. Baberschke, M. Donath, and W. Nolting (Springer, Berlin, 2001), p. 267.
[38] G. Hörmandinger, P. Weinberger, P. Marksteiner, and J. Redinger, Phys. Rev. B **38**, 1040 (1988).
[39] A. K. Rajagopal and J. Callaway, Phys. Rev. B **7**, 1912 (1973).
[40] M. V. Ramana and A. K. Rajagopal, Adv. Chem. Phys. **54**, 231 (1983).
[41] P. Strange, H. Ebert, and B. L. Gyorffy, J. Phys.: Condens. Matter **1**, 2959 (1989).
[42] O. K. Andersen, Phys. Rev. B **12**, 3060 (1975).
[43] O. K. Andersen and O. Jepsen, Phys. Rev. Lett. **53**, 2571 (1983).
[44] S. Picozzi, A. Continenza, and A. J. Freeman, Phys. Rev. B **66**, 094421 (2002).
[45] S. Picozzi, A. Continenza, and A. J. Freeman, Phys. Rev. B **69**, 094423 (2004).
[46] M. Magnuson, N. Wassdahl, and J. Nordgren, Phys. Rev. B **56**, 12238 (1997).
[47] V. Grebennikov, J. Electron Spectrosc. Relat. Phenom. **137-140**, 741 (2004).
[48] M. V. Yablonskikh, Y. M. Yarmoshenko, V. I. Grebennikov, E. Z. Kurmaev, S. M. Butorin, L.-C. Duda, J. Nordgren, S. Plogmann, and M. Neumann, Phys. Rev. B **63**, 235117 (2001).
[49] A. N. Titov, A. V. Kuranov, V. G. Pleschev, Y. M. Yarmoshenko, M. V. Yablonskikh, A. V. Postnikov, S. Plogmann, M. Neumann, A. V. Ezhov, and E. Z. Kurmaev, Phys. Rev. B **63**, 035106 (2001).
[50] M. V. Yablonskikh, Y. M. Yarmoshenko, I. V. Solovyev, E. Z. Kurmaev, L. C. Duda, T. Schmitt, M. Magnuson, J. Nordgren, and A. Moewes, J. Electron Spectrosc. Relat. Phenom. **144**, 765 (2005).
[51] T. Moria, *Spin Fluctuations in Magnetics* Vol. 32/c of Landolt-Börnstein Springer Series in Solid State Sciences, Group III (Springer-Verlag, Berlin, 2001), pp. 66–414.
[52] S. G. Chiuzbaian, G. Ghiringhelli, C. Dallera, M. Grioni, P. Amann, X. Wang, L. Braicovich, and L. Patthey, Phys. Rev. Lett. **95**, 197402 (2005).
[53] J. Kawai, C. Suzuki, and H. Adachi, J. Electron Spectrosc. Relat. Phenom. **78**, 79 (1996).
[54] A. Galtayries and J. Grimblot, J. Electron Spectrosc. Relat. Phenom. **99**, 267 (1999).
[55] J. Hafner and D. Hobbs, Phys. Rev. B **68**, 014408 (2003).
[56] D. Hobbs, J. Hafner, and D. Spisak, Phys. Rev. B **68**, 014407 (2003).
[57] L. Braicovich, G. Ghiringhelli, A. Tagliaferri, G. van der Laan, E. Annese, and N. B. Brookes, Phys. Rev. Lett. **95**, 267402 (2005).
[58] In the ground state of an atom the spin-flip of an electron is a result of thermal spin fluctuations (Ref. 51). Here we refer to the spin-flip of a single d electron as the process where it reverses its spin moment with respect to that before the excitation started (Ref. 52).